ELSEVIER

Catalysis Today 60 (2000) 193–207

CATALYSIS TODAY

www.elsevier.com/locate/cattod

Modification of faujasites to generate novel hosts for "ship-in-a-bottle" complexes

Carmen Schuster, Wolfgang F. Hölderich*

Department of Chemical Technology and Heterogeneous Catalysis, University of Technology RWTH Aachen, Worringerweg 1, 52074 Aachen, Germany

Abstract

Zeolites X, Y, and DAY have been modified by a post-synthetical dealumination procedure to generate mesopores that are completely surrounded by micropores. In these novel host materials several bulky transition metal salen complexes have been occluded via the "ship-in-a-bottle" synthesis approach. Both the host materials and the "ship-in-a-bottle" catalysts have been characterized by FTIR spectroscopy and nitrogen adsorption. Additionally, the "ship-in-a-bottle" catalysts have been characterized by thermogravimetric analysis and ICP-AES spectroscopy. The catalysts have been tested in the stereoselective epoxidation of *R*-(+)-limonene and (−)-α-pinene with molecular oxygen as oxidant. The best results so far — 100% conversion, 96% selectivity and 91% de — were achieved with the immobilized (*R*,*R*)-(*N*,*N*′)-bis(3,5-di-*tert*-butylsalicylidene)-1,2-diphenylethylene-1,2-diaminocobalt complex in the epoxidation of (−)-α-pinene.

Keywords: Dealumination; Mesopores; Catalysis; Oxidation; Olefin; Salen

1. Introduction

Due to the steadily increasing demand for optically pure compounds in the pharmaceutical and agrochemical field, the use of chiral catalysts has become a powerful tool in synthetic organic chemistry [1]. Numerous attempts have been made at the immobilization of homogeneous chiral catalysts [2–7]. In this regard, the "ship-in-a-bottle" approach dating back to 1977 offers several advantages over homogeneous or conventional heterogeneous catalytic systems where the metal complex is attached to a solid surface by covalent or ionic bonding [8,9]. The "ship-in-a-bottle" catalysts main feature is the host–guest interaction which is neither covalent nor ionic. The guest is retained in the zeolite matrix by restrictive pore openings and will, in principle, retain all properties of the homogeneous complex. The superiority of these catalysts to homogeneous systems is based on their easy separation from the reaction mixture and, thus, their recyclability and environmental compatibility [10]. Furthermore, it is likely that the zeolitic host bestows size and shape selectivity to the catalyst as well as a stabilizing effect on the organometallic complex since due to the site isolation of the single complexes multimolecular deactivation pathways such as formation of μ-oxo- or peroxo-bridged species will be rendered impossible [11,12]. However, even a large-pore zeolite such as zeolite Y, whose structure consists of almost spherical 13 Å supercages interconnected tetrahedrally through smaller apertures of 7.4 Å in diameter, is limited regarding the size of guest molecules by the space available in these cavities.

Our approach was to enlarge the intrazeolitic cavities in order to generate superior hosts for bulky homogeneous chiral catalysts. Such created mesopores

* Corresponding author. Tel.: +49-241-806560; fax: +49-241-8888291.
E-mail address: hoelderich@rwth-aachen.de (W.F. Hölderich)

0920-5861/00/$ – see front matter
PII: S0920-5861(00)00336-9

which are completely surrounded by micropores offer additional advantages: the entrapped metal complex can move freely and is more accessible during catalysis and even sterically demanding transition states can be formed within the individual pores. Such immobilized chiral transition metal complexes are used as catalysts in the stereoselective epoxidation of *R*-(+)-limonene and (−)-α-pinene.

2. Experimental

2.1. Materials

Zeolites NaY (Wessalith NaY) and DAY (Wessalith DAY) were kindly donated by Degussa-Hüls AG and zeolite NaX (SP7-8372) by Grace GmbH. Fluorobenzene (Fluka), *R*-(+)-limonene (Fluka), (−)-α-pinene (Aldrich) and pivalaldehyde (Aldrich) were purchased as reagent grade chemicals and were used without further purification.

2.2. Preparation of the host material

2.2.1. Parent material NaX or NaY

In a typical dealumination procedure, 10–15 g of zeolite X or Y (sodium form) in deep bed were dried at 723 K for 12 h under a steady flow of dry nitrogen (3 l/h) in a horizontal tubular quartz reactor with an internal diameter of 3 cm (heating rate: 5 K/min). The nitrogen stream was then saturated with silicon tetrachloride at room temperature and passed through the zeolite sample at 523 K for 1 h. After the $SiCl_4$-treatment was stopped the reactor was purged with nitrogen for several hours in order to remove residual silicon tetrachloride while the sample was allowed to cool to room temperature. The material was ion-exchanged three times with $(NH_4)CO_2CH_3$ and $(NH_4)Cl$ at 353 K for 24 h in order to replace sodium with ammonium. For the first ion-exchange a 10 M-ammonium acetate/2 M-ammonium chloride solution was used. The second and the third ion-exchanges were done using solely the 2 M-ammonium chloride solution. After washing and drying the zeolite was then treated in the same horizontal tubular quartz reactor with water vapor (nitrogen flow saturated with water at 353 K) at 873 K (heating rate: 5 K/min) for 3 h. After cooling to room temperature the zeolite sample was ion-exchanged with 2 M-ammonium chloride solution and treated with water vapor at 1123 K (heating rate: 10 K/min) for 3 h. Some of the extra-framework aluminum was removed by treatment with aqueous hydrochloric acid at pH 2.7 for 24 h at room temperature.

2.2.2. Parent material DAY

The DAY zeolite was ion-exchanged at 353 K for 24 h with 2 M-ammonium chloride solution prior to the hydrothermal treatment. 15–20 g of the ion-exchanged zeolite was then treated in a horizontal tubular quartz reactor (internal diameter: 3 cm) with water vapor (nitrogen flow saturated with water at 353 K) at 873 K (heating rate: 5 K/min) for 3 h. After cooling to room temperature the zeolite sample was ion-exchanged with 2 M-ammonium chloride solution and treated with water vapor at 1123 K (heating rate: 10 K/min) for 4.5 h. Sample CSZ135 has only been treated at 1123 K (heating rate: 10 K/min) for 6.5 h. Due to the low Al content of the parent DAY, the partial removal of the extraframework Al via acidic treatment was not necessary.

2.3. Catalyst preparation

To introduce the desired transition metal cation the zeolitic host was ion-exchanged for 24 h at 353 K with a solution of the corresponding transition metal salt. The ion-exchanged zeolite was then dried under vacuum at 823 K (heating rate: 1 K/min) and cooled under inert atmosphere prior to the synthesis of the salen ligands in the mesopores. The ligand synthesis was conducted at room temperature under an inert atmosphere. To the ion-exchanged zeolitic material was added an amount of the optically pure diamine in dichloromethane in slight excess (1.2 equiv.) to the metal content. After stirring for 24 h the appropriate amount of aldehyde in dichloromethane was added to the slurry and stirring was continued for another 24 h. The mixture was then transferred into an extraction thimble and was soxhlet-extracted with dichloromethane and toluene, respectively, until the solvent remained colorless.

2.4. Catalytic testing

The new immobilized salen complexes have been tested in the epoxidation of (*R*)-(+)-limonene and (−)-α-pinene according to Eqs. (1) and (2).

In a typical autoclave run 10 ml fluorobenzene, 1.85 mmol olefin ((*R*)-(+)-limonene or (−)-α-pinene) and 4.6 mmol pivalaldehyde were, quite similar to Mukaiyama et al. [13], added to 25 mg of catalyst at room temperature. After sealing the autoclave, 30 bar of oxygen were added and the reaction mixture was stirred vigorously. The reaction time was 24 h for (*R*)-(+)-limonene and 3 h for (−)-α-pinene.

The results of the catalytic testing are summarized in the figures. All experiments have been conducted twice.

2.5. Characterization

The wet chemical analysis was done on an Inductive Coupled Plasma Atomic Emission Spectroscopy (ICP-AES) Spectroflame D (Spectro). Typically, 30 mg sample was dissolved in 500 μl 40% HF-solution, 4 ml 1:4 H_2SO_4-solution and 45 ml H_2O.

For thermogravimetric analyses a Netzsch 209/2/E equipped with a STA 409 Controller was used. The heating rate was 2°C/min, using Al_2O_3-crucibles; α-Al_2O_3 was used as a reference material.

Fourier-transform infrared spectroscopy (FT-IR) was performed at room temperature on a Nicolet Spektrometer 460 Protégé using standard KBr techniques.

Nitrogen adsorption/desorption isotherms were obtained with a Micromeretics ASAP 2010 at 77 K. GC analysis was performed on a HP 6890 Series gas chromatograph (Hewlett–Packard) using a 60 m 1701 (CPSil 19) column and a 50 m FS-Cyclodex beta-I/P column.

3. Results and discussion

3.1. Dealumination procedure

For the generation of mesopores in the zeolitic framework, we subjected NaX and NaY zeolites to the combined dealumination steps with $SiCl_4$ and H_2O outlined in Scheme 1.

The dealumination procedure outlined in Scheme 1 leads to mesopores that are completely surrounded by microporous space. During treatment with silicon tetrachloride, a dealumination method first reported by Beyer et al. [14], the faujasite's framework aluminum is isomorphously replaced by silicon. The reaction is self-terminating due to the precipitation of $NaAlCl_4$ in the outer pores of the zeolite crystal [15]. The temperature we chose to conduct the reaction (523 K) is relatively mild. Therefore, it can be assumed that only the outer layers of the zeolite crystal are dealuminated by the treatment with $SiCl_4$.

During the successive ion-exchange the chloro aluminum complexes are extracted and the zeolite is converted into the ammonium form. The zeolite is then steam-dealuminated in a two-step procedure. The first steaming is carried out at 873 K and the second at 1123 K. Omission of the mild hydrothermal treatment at 873 K and proceeding directly to the treatment at 1123 K causes destruction of the zeolite structure. This could be due to the high amount of framework aluminum left within the crystal core after treatment with $SiCl_4$. After the first hydrothermal treatment in which the sample is heated quite care-

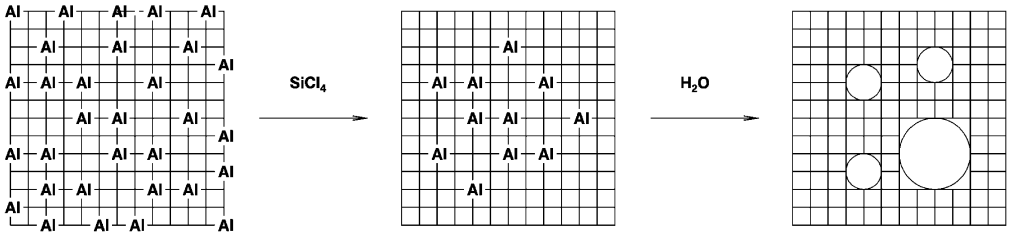

Scheme 1. Procedure to generate the novel host with mesopores completely surrounded by the micropores.

Table 1
Data of nitrogen adsorption and IR spectroscopy of the dealuminated zeolites and their parent materials

Sample	Parent material	T–O-symmetric stretch vibration (cm^{-1})	SiO_2/Al_2O_3	BET surface area (m^2/g)	*t*-Plot-milkroporous space (cm^3/g)	BJH-mesoporous volume (cm^3/g)
NaX		762	3.02	666.6	0.307	0.044
CHZ22SB	NaX	835	125.11	346.2	0.132	0.183
CHZ104SB	NaX	836	188.67	343.9	0.122	0.188
NaY		794	6.67	720.4	0.329	0.036
CHZ90SB	NaY	836	188.67	611.6	0.251	0.176
CHZ94SB	NaY	836	188.67	597.3	0.245	0.165
DAY		836	188.67	663.5	0.284	0.078
CSZ128	DAY	837.5	760.66	597.3	0.254	0.097
CSZ135	DAY	837.7	1269.10	595	0.253	0.09

fully (5 K/min) to 873 K, this amount of framework aluminum has considerably decreased. Therefore, in the second steaming step the sample can be heated more quickly (10 K/min) to a much higher temperature (1123 K) without collapse of the zeolite structure. After the second hydrothermal treatment at 1123 K, a high degree of dealumination has been achieved with a SiO_2/Al_2O_3 ratio ranging from 125.1 to 188.7 for both zeolites X and Y (Table 1).

Using the described dealumination procedure over all steps, highly dealuminated faujasite zeolites are obtained regardless of the parent material. Materials with a SiO_2/Al_2O_3 ratio above 380 can be synthesized by subjecting the DAY zeolite to hydrothermal treatment at high temperatures (Table 1).

Final treatment of the host material with hydrochloric acid removes some of the extra-framework aluminum in order to make room for guest molecules. Complete removal of the extra-framework aluminum species renders the zeolite less stable under alkaline and hydrothermal conditions and leads to a collapse of the zeolite structure [16,17].

3.2. Characterization of the host materials

The progress of the dealumination is followed by IR spectroscopy. Fig. 1 shows the IR spectra of zeolite Y taken between the different dealumination steps. The labeled bands indicate the framework sensitive external symmetric stretch assigned to an Al–O vibration [16,18]. The shift of this vibration towards higher wavenumbers is directly linked to the decrease in framework aluminum and can therefore be used to quantify the amount of framework aluminum left after each step of the dealumination procedure. The parent material, having its band at 794 cm^{-1}, has a SiO_2/Al_2O_3 ratio of 6.67. After treatment with $SiCl_4$ the band has shifted to 817 cm^{-1}, which is equal to a SiO_2/Al_2O_3 ratio of 16.16. The first steaming at 873 K shifts the external symmetric stretch to 829 cm^{-1}, increasing the SiO_2/Al_2O_3 ratio to 40.37. After the second steaming at 1123 K the band has shifted to 836 cm^{-1}, resulting in a SiO_2/Al_2O_3 ratio of 188.67 (see also Table 1). The final treatment, the acidic leaching to remove extra-framework aluminum generated during steaming, does not lead to a further dealumination of the zeolite lattice.

The highly dealuminated hosts and their corresponding parent materials have been characterized by nitrogen adsorption and IR spectroscopy prior to occlusion of the guest molecules. The results are presented in Table 1. For each of the parent zeolites two typical dealumination examples are listed below their respective starting materials.

Figs. 2–4 show the BET plots of dealuminated zeolites X, Y, and DAY and their respective parent materials. The isotherms of the dealuminated zeolites exhibit the characteristics of a mixed micro/mesoporous material, i.e. the hysteresis loop in the high pressure region typical for the presence of mesopores and the reversible isotherm with its steep adsorption in the low pressure region that is typical for microporous materials. According to Fajula et al. [19,20] who have obtained similar BET plots for steamed zeolites omega and mazzite, the steep nitrogen desorption in the region of p/p_0 0.4–0.5 indicates mesopores with

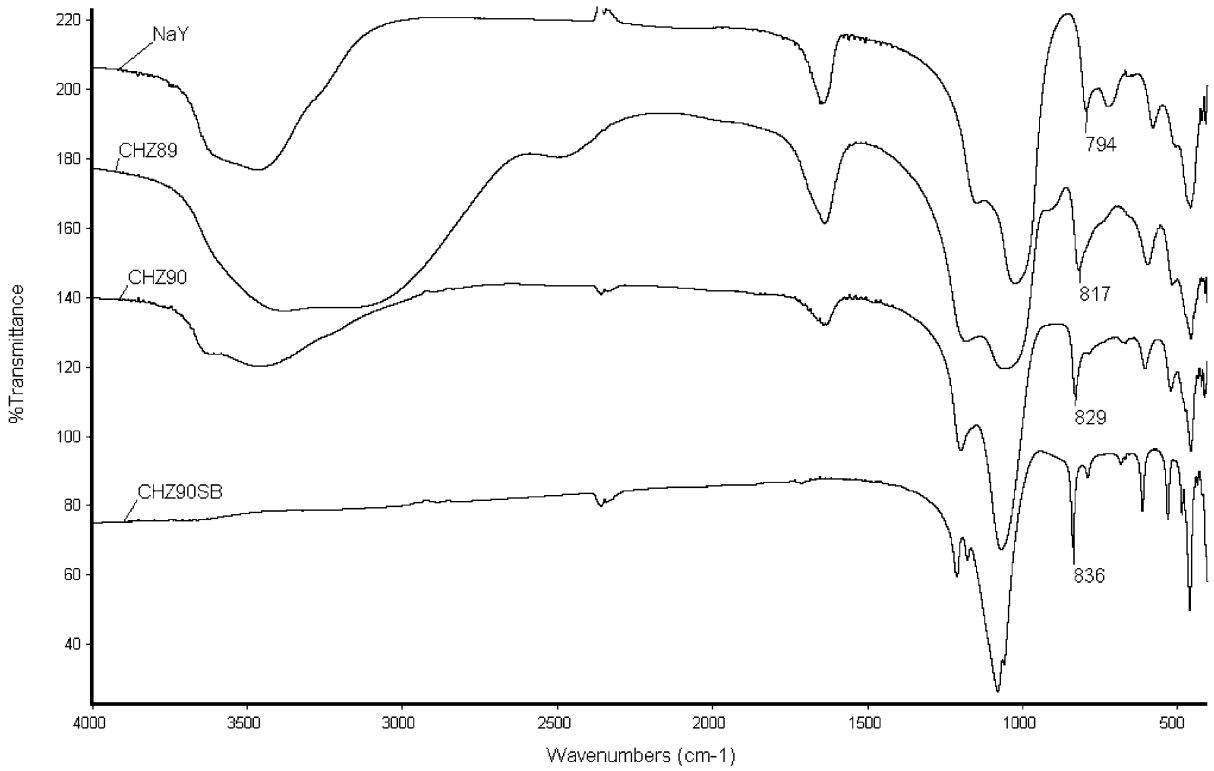

Fig. 1. IR spectra of zeolite Y: parent material (NaY), after $SiCl_4$ treatment (CHZ89), after the first steaming at 873 K (CHZ90) and after the second steaming at 1123 K (CHZ90SB).

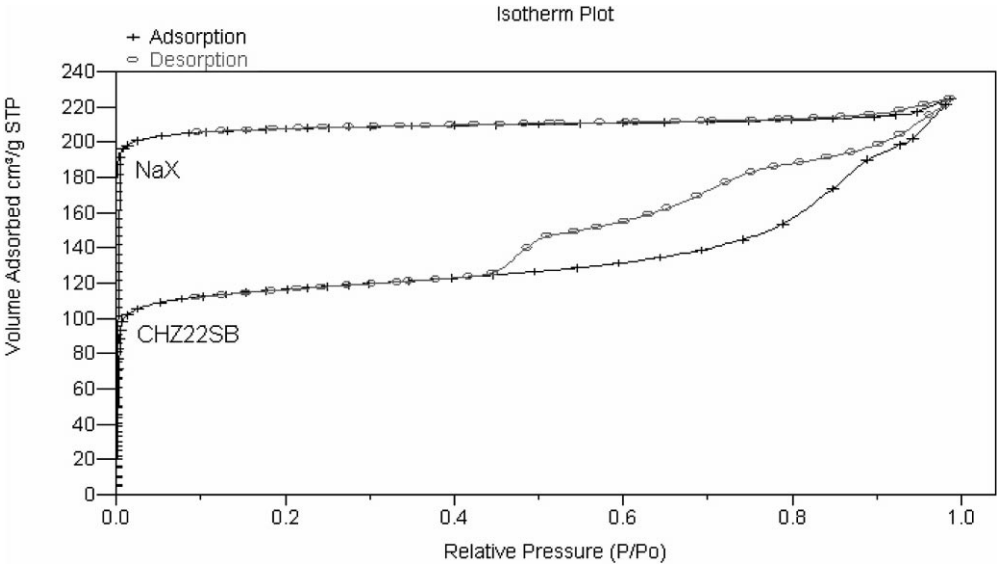

Fig. 2. Nitrogen adsorption characteristics of the dealuminated zeolite X (CHZ22SB) and its parent material.

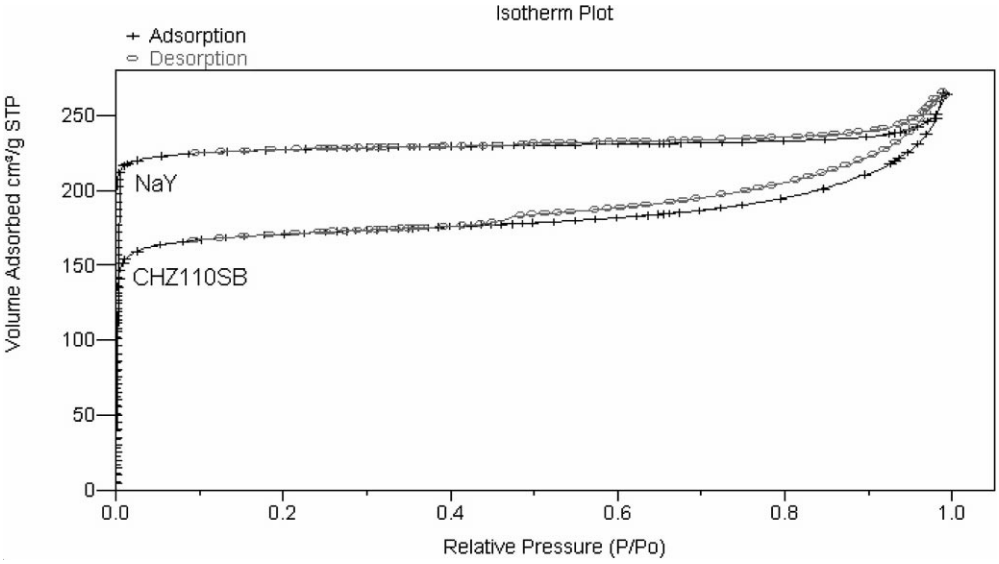

Fig. 3. Nitrogen adsorption characteristics of the dealuminated zeolite Y (CHZ110SB) and its parent material.

ink-bottle openings. For the steamed zeolite mazzite those mesopores are described to be connected to the crystal surface by necks smaller than 4 nm in diameter [20]. Comparison of Figs. 2–4 show the influence of the framework composition on the result of the dealumination. Zeolite X, having the highest Al content of the starting materials (see Table 1), suffers the gravest loss of BET surface area and microporous space upon dealumination. Zeolite Y loses considerably less of its BET surface area and microporous space and zeolite DAY hardly loses any at all. However, zeolite X also gains the largest amount of mesoporous space of the

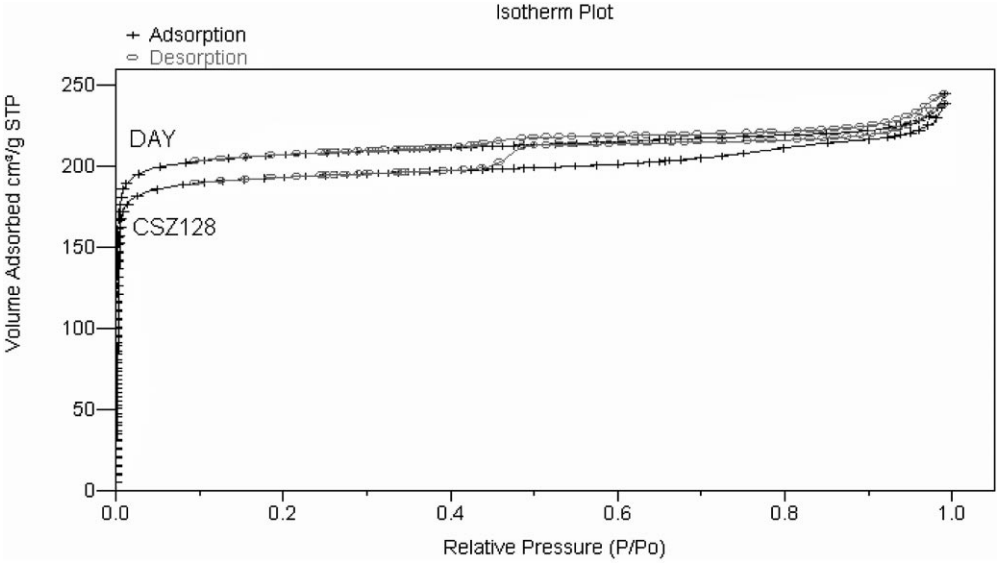

Fig. 4. Nitrogen adsorption characteristics of the dealuminated zeolite DAY (CSZ128) and its parent material.

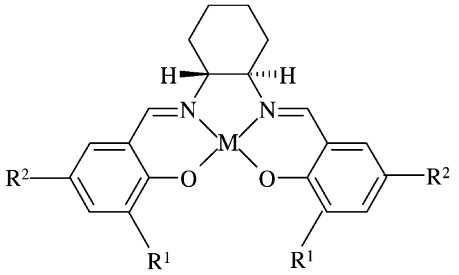

salen-**1**: R^1 = H, R^2 = H
salen-**2**: R^1 = t-Bu, R^2 = t-Bu
salen-**3**: R^1 = t-Bu, R^2 = Me
salen-**4**: R^1 = t-Bu, R^2 = H

Fig. 5. Salen complexes based on (*R*,*R*)-cyclohexanediamin (salen-1: R^1=H, R^2=H; salen-2: R^1=*t*-Bu, R^2=*t*-Bu; salen-3: R^1=*t*-Bu, R^2=Me; salen-4: R^1=*t*-Bu, R^2=H).

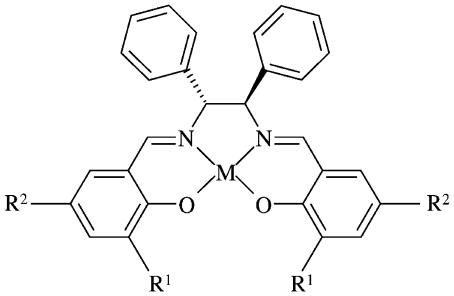

salen-**5**: R^1 = t-Bu, R^2 = t-Bu
salen-**6**: R^1 = t-Bu, R^2 = Me
salen-**7**: R^1 = t-Bu, R^2 = H

Fig. 6. Salen complexes based on (*R*,*R*)-diphenylethylendiamin (salen-5: R^1=*t*-Bu, R^2=*t*-Bu; salen-6: R^1=*t*-Bu, R^2=Me; salen-7: R^1=*t*-Bu, R^2=H).

three dealuminated materials whereas zeolite DAY, having the lowest Al content of the starting materials (see Table 1), obtains the least mesoporous volume upon dealumination.

3.3. Immobilization procedure

Molecular modeling predicts, e.g. that Jacobsen's catalyst *N*,*N*′-bis(3,5-di-*tert*-butylsalicylidene)-1,2-cyclohexanediaminomanganese chloride, due to its four bulky *tert*-butyl groups, does not fit into the Y zeolite supercages [7,21]. Therefore, our target molecules for the entrapment in the novel host material were Jacobsen's catalyst and equally or even more sterically demanding transition metal salen complexes. Figs. 5 and 6 show the salen complexes that have been entrapped in the mesopores of the new host materials.

3.4. Characterization of the immobilized complexes

In Fig. 7 the FT-IR spectra of the salen-2 ligand (A), the Jacobsen catalyst (B) and immobilized Jacobsen catalyst (C) are compared. Whereas spectra A and B were obtained using standard KBr techniques, the "ship-in-a-bottle" catalyst (C) was prepared as a self-supporting wafer. The characteristic band of the complex (*) at 1535 cm^{-1} can only be found in spectra B and C. These results are in accordance with data published earlier for the zeolite-occluded (*R*,*R*)-(*N*,*N*′)-bissalicylidene-1,2-cyclohexanediaminato(2-) manganese(III) complex [7], i.e. Jacobsen's catalyst without its four tertiary butyl groups, and for the zeolite-entrapped cobalt(II) and platinum(II) complexes of (*R*,*R*)-(*N*,*N*′)-bissalicylidene-1,2-cyclohexanediamine [21]. This can be considered as proof of the presence of Jacobsen's catalyst, [(*R*,*R*)-(*N*,*N*′)-bis(3,5-di-*tert*-butylsalicylidene)-1,2-cyclohexanediaminato(2-)-manganese(III)]$^+$, in our "ship-in-a-bottle" catalyst.

Fig. 8 shows the analogous FT-IR spectra for the salen-5 ligand (A), the homogeneous Co(salen-5) complex (B) and immobilized Co(salen-5) complex (C). In agreement with the results obtained in the comparison of the three spectra in Fig. 7 the characteristic band of the complex (*) can also be found only in the spectra of the homogeneous and immobilized Co(salen-5) complexes (B) and (C), respectively, and not in the spectrum of the pure ligand (A). That can be considered as proof of the successful occlusion of the even more bulky Co(salen-5) complex in our host material.

The metal and ligand contents of the "ship-in-a-bottle" catalysts have been determined by wet chemical analysis and thermogravimetric analysis, respectively. The results, as summarized in Table 2, sug-

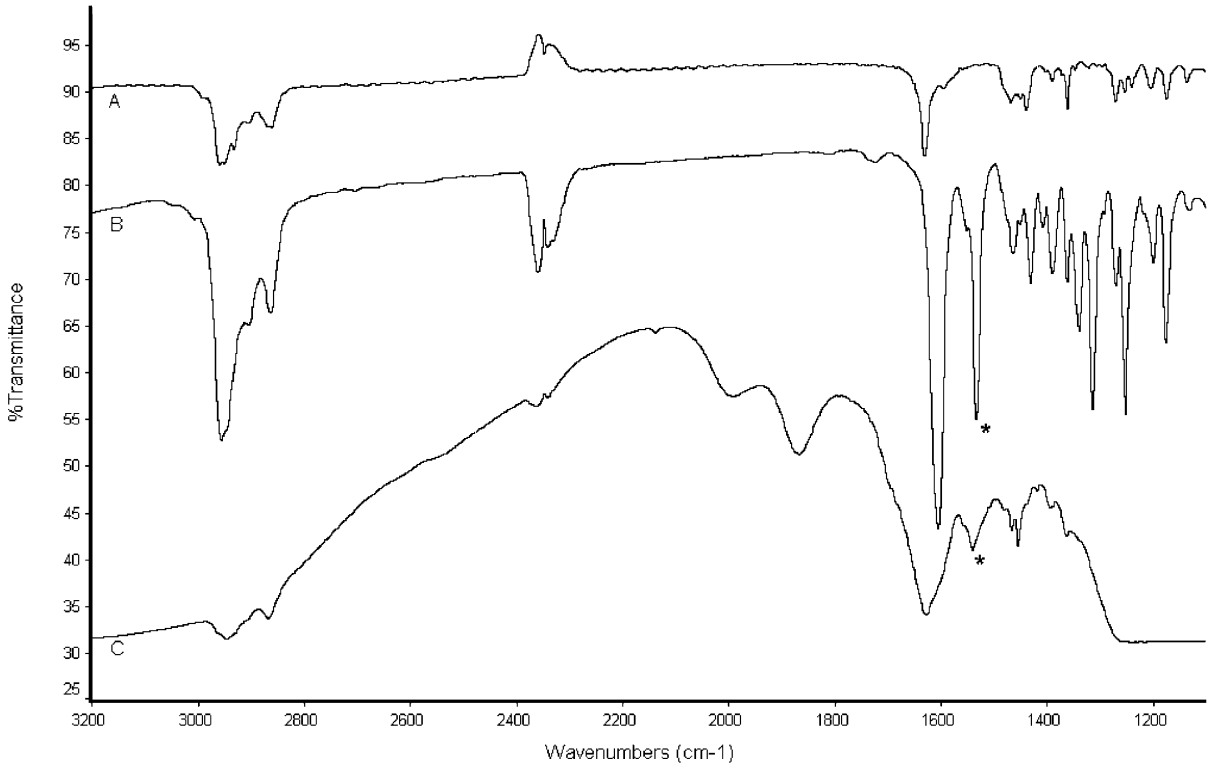

Fig. 7. FT-IR spectra of the salen-2 ligand (A), the Jacobsen catalyst (B) and the immobilized Jacobsen catalyst (C), (*) absorption characteristic of the complex.

gest that the metal to ligand ratios follow no distinctive pattern. Only in the Mn(salen-3) and Mn(salen-4) catalysts the amount of ligand is equimolar to the manganese loading. About half of the other catalysts show an excess of metal with regard to the ligand content. The other half show an excess of ligand regarding the metal loading. Due to problems with the ICP-AES apparatus, the Ir content of the Ir(salen-5) catalyst has not been determined. All host materials listed in Table 2 have been prepared according to the procedure described in Section 2. Their properties are similar to those of the examples given in Table 1.

In order to investigate the location of the transition metal salen complexes within the host material, we conducted nitrogen adsorption experiments with the empty zeolitic host and with three different immobilized Mn salen complexes. The results are summarized in Table 3. In comparison to the host material, a decrease in the BET surface area and the micro- and mesoporous volumes can be detected with all three "ship-in-a-bottle" catalysts. For the Mn(salen-1)SIB catalyst, which hosts the smallest among the three entrapped organometallic compounds, the decrease of microporous space is the most prominent, indicating that this complex is mainly located in the zeolite's micropores. In contrast, the Mn(salen-5) complex, the most bulky of the guest molecules, seems to occupy mainly the mesoporous space of its host. According to the nitrogen adsorption data of the Mn(salen-2)SIB catalyst, the guest occupies both micropores and mesopores of the host material, suggesting that major parts of the ligands, e.g. the *tertiary*-butyl-substituted aromatic groups, stick through the intrazeolitic openings into the microporous space.

Fig. 9 should be understood as a very simplified model to depict schematically the entrapment of an organometallic guest molecule in the mesopores of the novel host material. In accordance with the observa-

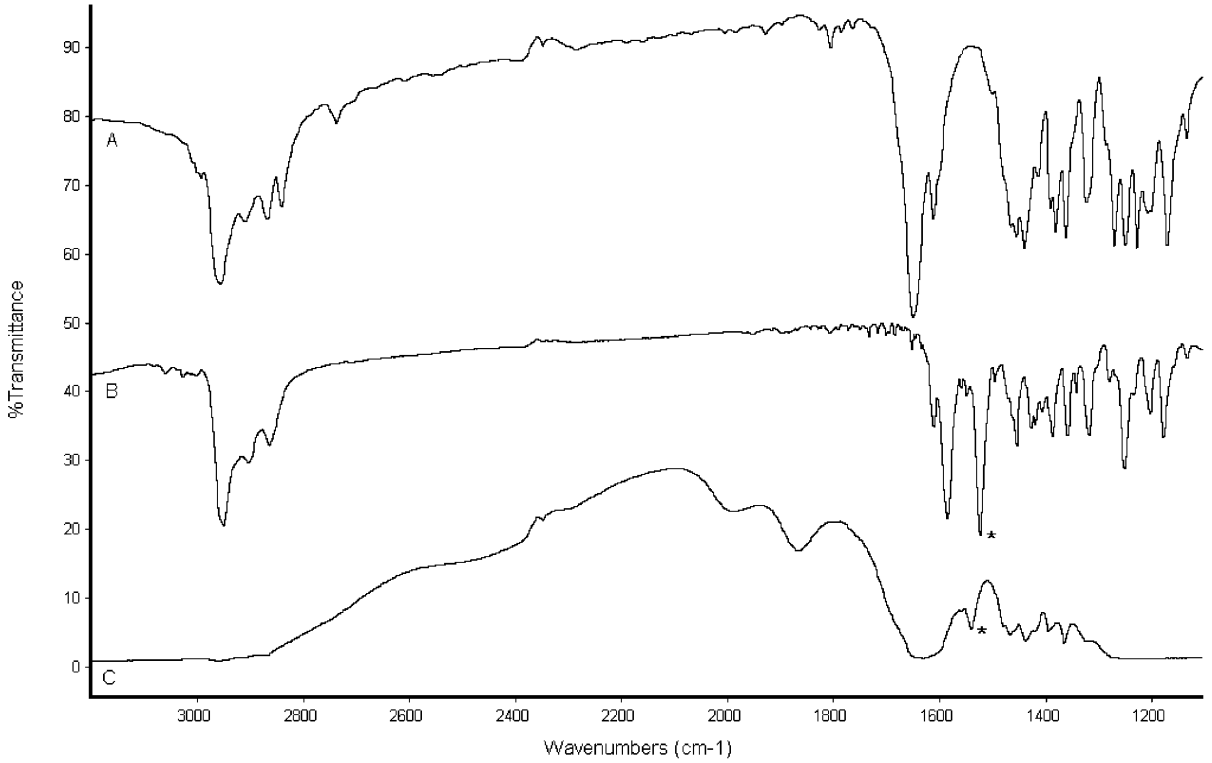

Fig. 8. FT-IR spectra of the salen-5 ligand (A), the homogeneous Co(salen-5) complex (B) and the immobilized Co(salen-5) complex (C), (*) absorption characteristic of the complex.

Table 2
Data of catalyst characterization

Catalyst	Metal content (wt.%)	Ligand content (wt.%)	Host/type of parent material
Mn(salen-1)	0.35	2.8	CSZ135/DAY
V(salen-2)	0.96	3.7	CSZ133/DAY
Cr(salen-2)	0.61	5.8	CSZ110SB/NaY
Mn(salen-2)	0.49	6.4	CHZ106SB/NaY
Fe(salen-2)	0.11	5.0	CSZ135/DAY
Co(salen-2)	0.14	5.8	CHZ90SB/NaY
Mn(salen-3)	0.55	5.3	CHZ88SB/NaY
Mn(salen-4)	0.52	3.9	CHZ92SB/NaY
Cr(salen-5)	1.10	6.0	CHZ118SB/NaX
Mn(salen-5)	0.79	2.4	CSZ129/DAY
Fe(salen-5)	1.37	5.7	CHZ118SB/NaX
Co(salen-5)	0.29	8.0	CHZ104SB/NaX
Rh(salen-5)	0.43	12.2	CHZ112SB/NaY
Ir(salen-5)	n.d.	2.2	CSZ129/DAY
Mn(salen-6)	0.38	1.7	CSZ135/DAY
Mn(salen-7)	0.36	2.2	CSZ135/DAY

tions published earlier by Fajula et al. [19,20], we assume that the mesopores generated by our dealumination sequence are connected to each other and to the crystal surface via the three-dimensional microporous intrazeolite channel system.

3.5. Epoxidation of R-(+)-limonene

These catalysts have been tested in the stereoselective epoxidation of *R*-(+)-limonene and (−)-α-pinene

Table 3
Nitrogen adsorption investigations

Sample	BET surface area (m^2/g)	*t*-Plot microporous volume (cm^3/g)	BJH-mesoporous volume (cm^3/g)
Host (CHZ129)	522.2	0.211	0.113
Mn(salen-1)SIB	393.0	0.153	0.102
Mn(salen-2)SIB	396.2	0.158	0.098
Mn(salen-5)SIB	373.7	0.166	0.064

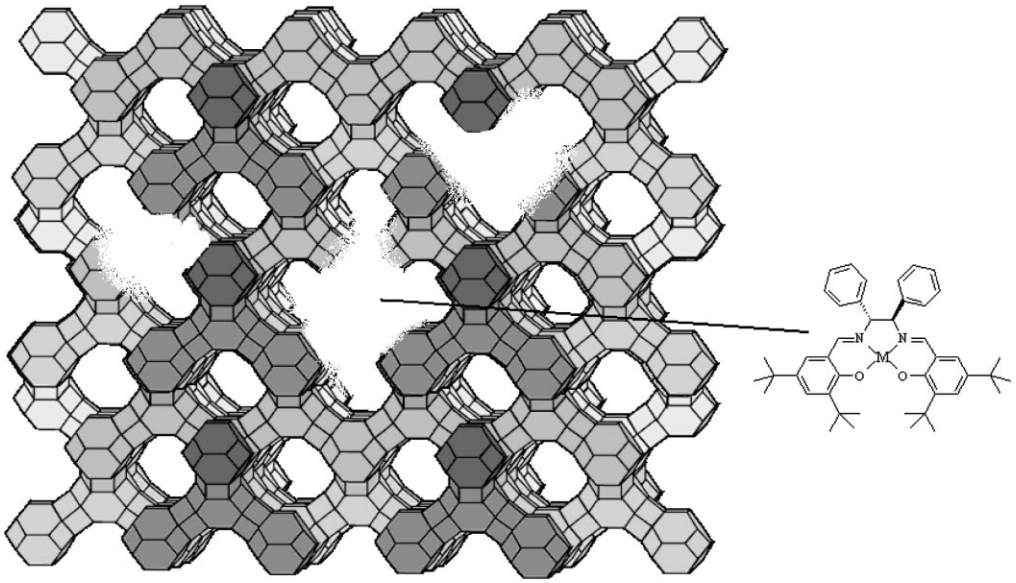

Fig. 9. Model of a M(salen-5) complex entrapped in mesopores that are completely surrounded by micropores.

(Section 3.6) according to Eqs. (1) and (2). The catalytic system applied in the test reactions is somewhat similar to the one introduced by Mukaiyama et al. [13] and was favored over the system used by Jacobsen et al. [22]. The main reason for not using Jacobsen's system is the fact that it does not work properly with the new heterogeneous catalysts. Upon occlusion of the transition metal salen complexes in the zeolitic hosts, the original 2-phase system (organic layer containing the catalyst and the olefin/aqueous layer containing the oxidant NaOCl) becomes a 3-phase system (organic layer containing the olefin/aqueous NaOCl-layer/solid catalyst) in which the catalyst is located at the bottom of the reaction vessel. No amount of stirring results in a satisfactory mixing of the phases to establish sufficient contact between catalyst, olefin and oxidant. Furthermore, one of the benefits of the system described in this work is that undesirable salt formation can be avoided by the use of environmentally benign molecular oxygen instead of sodium hypochloride as oxidant. Due to its inert nature and the excellent solubility of molecular oxygen in fluorous solvents fluorobenzene has been chosen as solvent. Besides, the combination of a transition metal, an organic ligand and a reductant creates an effective oxygenation system in an aerobic reaction [23].

Oxidation of R-(+)-limonene:

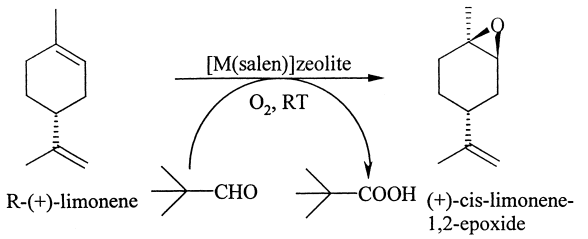

(1)

In order to investigate if the homogeneous complexes retained their catalytic activity upon their immobilization in our new hosts, we tested several of the immobilized complexes and their homogeneous counterparts in the oxidation of *R*-(+)-limonene according to Eq. (1).

The results, as summarized in Fig. 10, show that in general the organometallic complexes have been immobilized without considerable loss of catalytic activity. With exception of the Co(salen-2) complex all catalysts retained their catalytic properties upon entrapment in the host materials. The catalytic results achieved in the epoxidation of *R*-(+)-limonene with both the homogeneous and heterogeneous (salen-2)

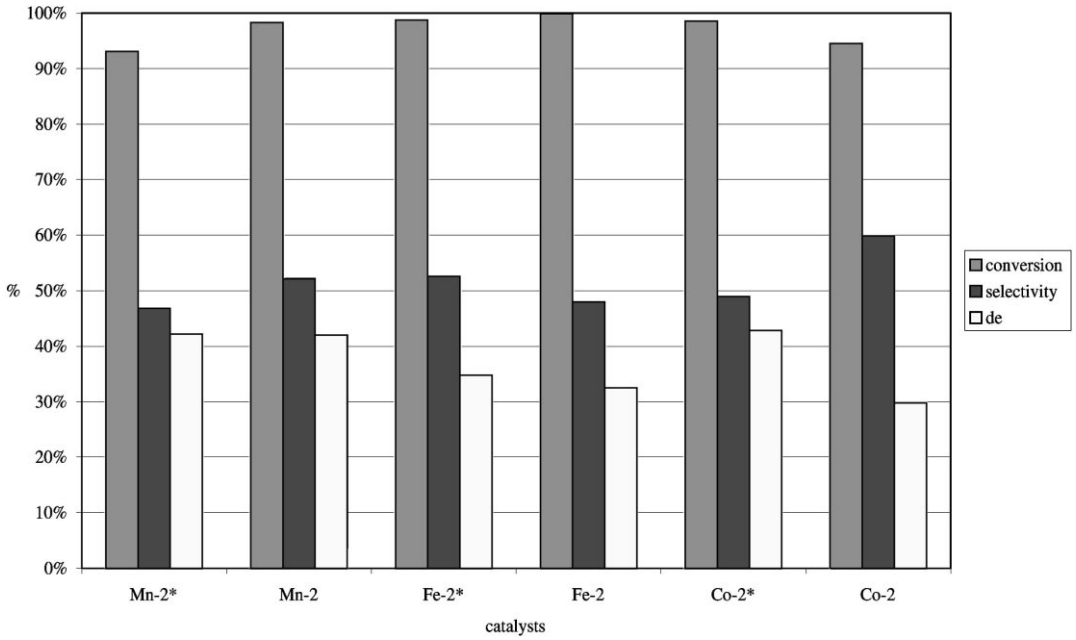

Fig. 10. Epoxidation of *R*-(+)-limonene in the presence of various homogeneous and immobilized transition metal (salen-2) complexes, (*) homogeneous complex.

complexes are quite similar to each other, regardless of the nature of metals.

We investigated the progress of the *R*-(+)-limonene epoxidation with regard to the reaction time by taking samples in intervals of 5 min. The results of this study, as depicted in Fig. 11, suggest that after 50–60 min the reaction has reached its equilibrium. A final sample which was taken after 24 h confirmed that indeed no further reaction could be detected.

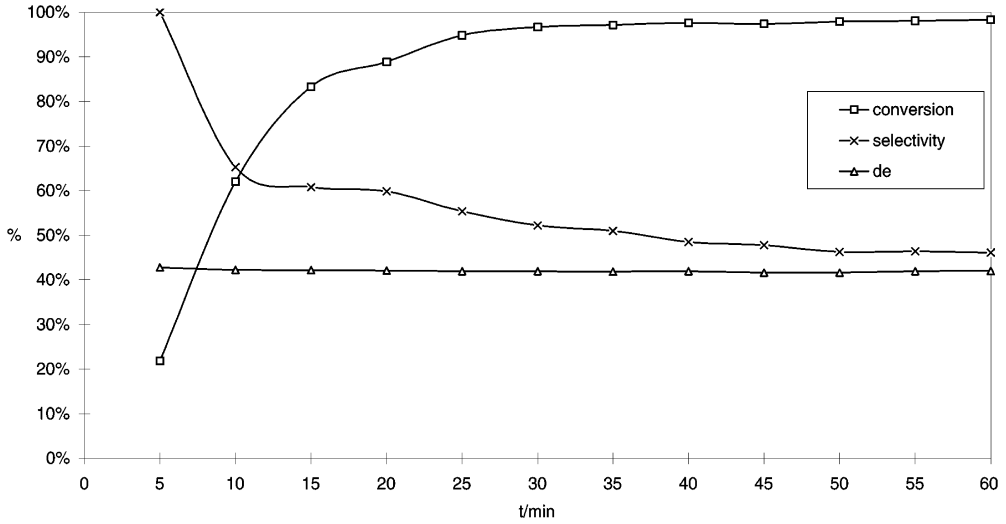

Fig. 11. Progress of the limonene epoxidation with regard to the reaction time.

Table 4
Effect of oxygen pressure in the epoxidation of *R*-(+)-limonene

Oxygen pressure (bar)	Conversion (%)	Selectivity (%)	de (%)
10	93	70	40
20	95	66	41
30	99	46	41
40	100	45	41

After having investigated the progress of the *R*-(+)-limonene epoxidation with regard to the reaction time (Fig. 11), we studied the influence of oxygen pressure on the system. At atmospheric pressure the system did not work properly, because due to the lack of pressure the oxygen uptake of the solution was erratic and the catalytic results could not be reproduced. Therefore, the epoxidation of *R*-(+)-limonene was conducted with 10, 20, 30 (standard procedure, see Section 2), and 40 bar of oxygen. The results, as summarized in Table 4, show that epoxide selectivities increased with decreasing oxygen pressure. The stereoselectivity of the reaction remained stable throughout the pressure experiments, indicating that the entrapped organometallic complex is not afflicted by a change in pressure. The best results of this study — 70% selectivity at 90% conversion and 40% de — were achieved with 10 bar of oxygen pressure. However, increasing the oxygen pressure from the standard pressure of 30 bar up to 40 bar did not lead to a further decrease in epoxide selectivity.

The aspect of catalyst reuse was studied by recycling of the immobilized Mn(salen-2) complex in the epoxidation of *R*-(+)-limonene according to Eq. (1). After each run the "ship-in-a-bottle" catalyst was separated by filtration from the reaction mixture and rinsed thoroughly with fluorobenzene. The solid was air-dried prior to reuse. The results, as shown in Table 5, demonstrate that the new heterogeneous catalysts can be reused at least twice without considerable loss of catalytic activity and selectivity.

Table 5
Reuse of the immobilized Mn(salen-2) complex in the epoxidation of *R*-(+)-limonene

Run	Conversion (%)	Selectivity (%)	de (%)
1	98	51	41
2	96	48	42
3	99	52	42

In order to investigate if our zeolite contributes to the product spectrum beside serving as host to the active compound, we conducted several catalytic experiments with the unloaded dealuminated zeolites as well as with the manganese-exchanged material prior to ligand synthesis. According to GC analysis no reaction took place. However, the presence of isolated acidic sides within the cavities of the dealuminated zeolites and the possibility of their interaction with the transition metal complex during catalysis cannot be completely ruled out.

3.6. Epoxidation of (−)-α-pinene

Similar to the epoxidation of *R*-(+)-limonene, we investigated our catalysts' behavior in the epoxidation of (−)-α-pinene according to Eq. (2). The results are summarized in Figs. 12–14.

Oxidation of (−)-α-pinene:

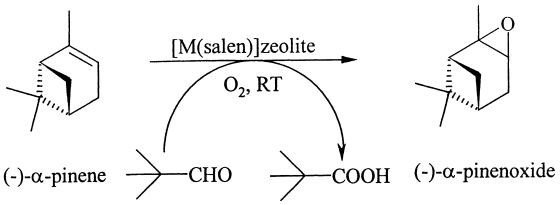

(2)

Fig. 12 shows that the (salen-2) complexes of Fe and V and the Co(salen-5) complex retained their catalytic properties upon entrapment in the host materials. In contrast to the Mn(salen-2) complex which loses only some of its epoxide selectivity upon immobilization, the corresponding Co and Cr complexes show an additional decrease in stereoselectivity as well. Strikingly, the immobilized Co(salen-5) complex achieved with 100% conversion, 96% selectivity and 91% de even better results in the epoxidation of (−)-α-pinene than its homogeneous counterpart. However, it is worth noting that among the (salen-2) complexes neither the homogeneous nor the occluded Jacobsen complex catalyzed the epoxidation of (−)-α-pinene best within their respective groups. In contrast to the epoxidation of *R*-(+)-limonene depicted in Fig. 10, an influence of the transition metal can be observed in the epoxidation

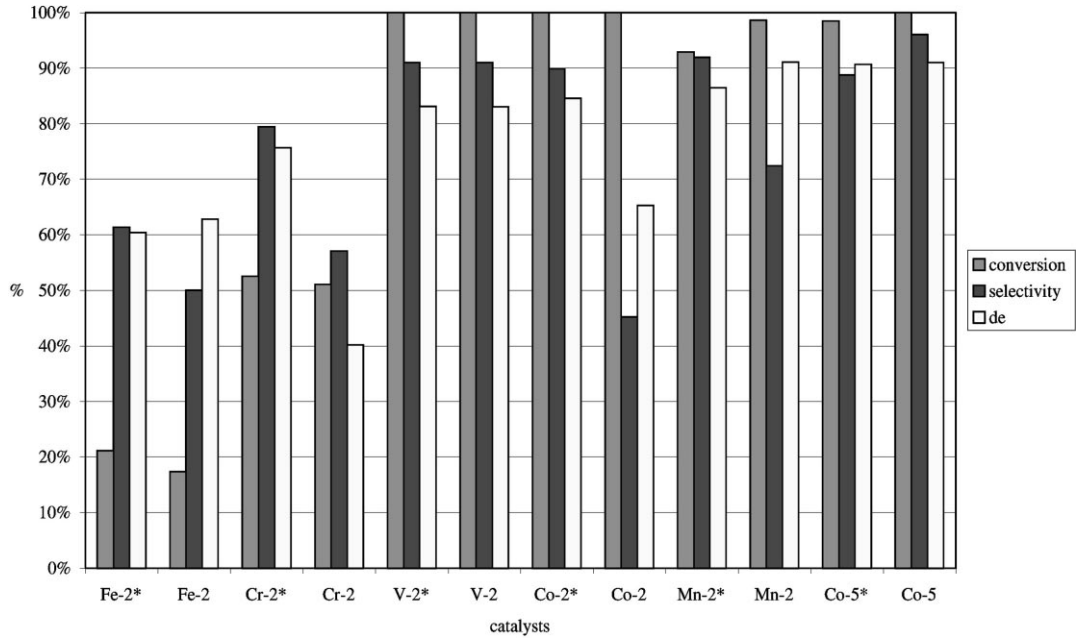

Fig. 12. Epoxidation of (−)-α-pinene in the presence of various homogeneous and immobilized transition metal (salen) complexes, (*) homogeneous complex.

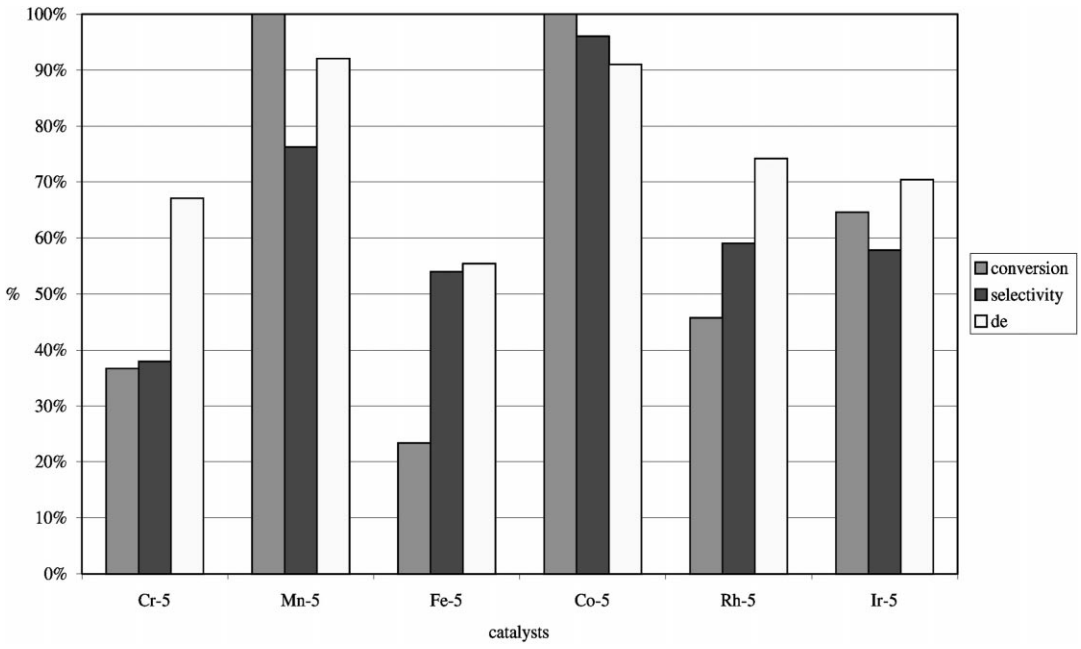

Fig. 13. Epoxidation of (−)-α-pinene in the presence of various immobilized transition metal (salen-5) complexes.

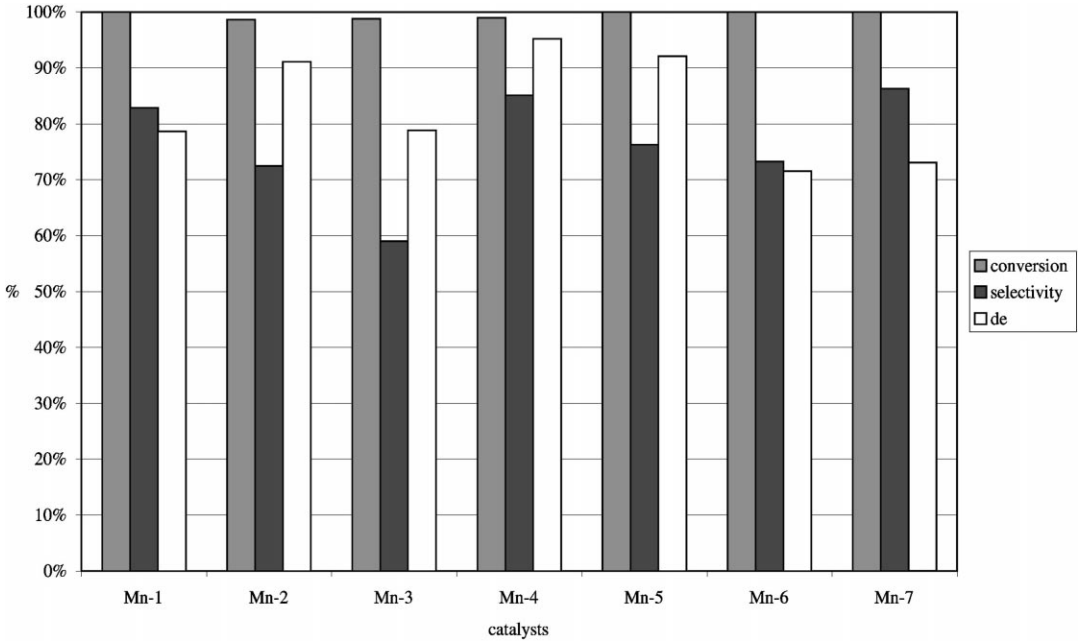

Fig. 14. Epoxidation of (−)-α-pinene in the presence of various immobilized Mn(salen) complexes.

of (−)-α-pinene for quite different catalytic results are obtained with the different (salen-2) complexes.

Due to the excellent catalytic results obtained in the epoxidation of (−)-α-pinene with the immobilized Co(salen-5) complex (Fig. 12), we entrapped a variety of transition metal complexes of the salen-5 ligand and investigated their catalytic behavior under the same reaction conditions. The results, as depicted in Fig. 13, indicate that except for the Co(salen-5) complex only the corresponding manganese complex exhibits promising potential. The (salen-5) complexes of Cr and Fe, others gave only modest conversion and all catalysts, with the exception of the Co and Mn species achieved, at the very best, moderate product and stereoselectivities.

We studied the catalytic behavior of seven different entrapped Mn(salen) complexes (Figs. 5 and 6) in the epoxidation of (−)-α-pinene, too. The results, as summarized in Fig. 14, show that all catalysts achieved high conversion (>95%). Surprisingly, with regard to product and stereoselectivity, the best results of this study were obtained with the immobilized manganese complexes of salen-4 and salen-5 and not, as one might expect, with the occluded Jacobsen catalyst Mn(salen-2). Taking into consideration the observations made in the discussion of Fig. 12, i.e. neither the homogeneous nor the immobilized Jacobsen complex achieved the best catalytic results among their respective (salen-2) counterparts, it can be assumed that Jacobsen's catalyst is not particularly suited for the epoxidation of (−)-α-pinene.

To establish the lack of leaching of the complex, we performed chemical analysis of the liquid after reaction. No metal ions could be detected. We further investigated the aspect of leaching as suggested by Sheldon et al. [24] by separating the catalyst from the reaction mixture by filtration prior to total olefin consumption. The filtrate was stirred additionally for several hours under reaction conditions. According to GC analysis no further reaction had occurred after filtration of the "ship-in-a-bottle" catalyst.

4. Conclusion

Zeolites X and Y have been highly dealuminated by a succession of different dealumination methods, i.e. dealumination by treatment with $SiCl_4$ and

dealumination by steaming, generating mesopores which are completely surrounded by microporous space. The same type of mesopores have been generated in aluminum-poor zeolite DAY upon hydrothermal treatment. This could be proved by the occlusion of several bulky transition metal salen complexes via the "ship-in-a-bottle" synthesis method and by means of nitrogen adsorption and FT-IR spectroscopy.

These "ship-in-a-bottle" catalysts have been characterized by means of nitrogen adsorption measurements and IR spectroscopy. The catalytic behavior of the entrapped bulky transition metal complexes has been investigated in the stereoselective epoxidation of *R*-(+)-limonene and (−)-α-pinene. A comparison of the respective catalytical results of the new heterogeneous catalysts and their homogeneous counterparts showed that the entrapment of the organometallic complex was achieved without considerable loss of activity and selectivity. The immobilized catalysts are reusable and do not leach. The best results so far — 100% conversion, 96% selectivity and 91% de — were achieved with the immobilized Cobalt(salen-5) complex in the epoxidation of (−)-α-pinene.

Acknowledgements

We are very grateful to the Deutsche Forschungsgemeinschaft (DFG), Sonderforschungsbereich 380, for their financial support of this work.

References

[1] R.A. Sheldon, Chirotechnology: Industrial Synthesis of Optically Active Compounds, Marcel Dekker, New York, 1993.
[2] G.J. Kim, S.H. Kim, Catal. Lett. 57 (1999) 139.
[3] J.A. Mayoral, J.M. Fraile, J.I. Carcía, J. Massam, J. Mol. Catal. A 136 (1998) 47.
[4] P. Piaggio, P. McMorn, C. Langham, D. Bethell, P.C. Bulman-Page, F.E. Hancock, G.J. Hutchings, New J. Chem. 22 (1998) 1167.
[5] I.F.J. Vankelecom, D. Tas, R.F. Parton, V. Van de Vyver, P.A. Jacobs, Angew. Chem. 108 (1996) 1445.
[6] A. Corma, M. Iglesias, F. Mohino, F. Sánchez, J. Organomet. Chem. 544 (1997) 147.
[7] A. Corma, M.J. Sabater, A. Domenech, V. Fornés, H. García, Chem. Commun. (1997) 1285.
[8] V.Y. Zakharov, B.V. Romanovsky, Vestn. Mosk. Univ. Khim. 18 (1977) 142.
[9] G. Schulz-Ekloff, G. Meyer, D. Wöhrle, M. Mohl, Zeolites 4 (1984) 30.
[10] P.A. Jacobs, R. Parton, D. de Vos, Enzyme mimicking with zeolites, in: Zeolite Microporous Solids: Synthesis, Structure, and Reactivity, Kluwer Academic Publishers, Dordrecht, 1992, p. 555.
[11] K.J. Balkus Jr., A.K. Khanmamedova, K.M. Dixon, F. Bedioui, Appl. Catal. A 143 (1996) 159.
[12] W.F. Hölderich, C. Heinrichs, Catal. Lett. 58 (1999) 75.
[13] T. Mukaiyama, T. Yamada, K. Imagawa, T. Nagata, Chem. Lett. 11 (1992) 2231.
[14] H.K. Beyer, I.M. Belenykaja, Stud. Surf. Sci. Catal. 5 (1980) 203.
[15] H.K. Beyer, P.J. Grobet, P.A. Jacobs, Zeolites 6 (1986) 47.
[16] J. Klinowski, M.W. Anderson, J. Chem. Soc., Faraday Trans. 1 (82) (1986) 1449.
[17] W. Lutz, E. Löffler, B. Zibrowius, Stud. Surf. Sci. Catal. 97 (1995) 327.
[18] J.R. Sohn, S.J. DeCanio, Zeolites 6 (1986) 225.
[19] F. Fajula, B. Chauvin, P. Massiani, R. Dutartre, F. Figueras, T. Des Courieres, Zeolites 10 (1990) 174.
[20] F. Fajula, R. Dutartre, L.C. de Ménorval, F. Di Renzo, D. McQueen, P. Schulz, Micropor. Mater. 6 (1996) 311.
[21] W.F. Hölderich, W. Kahlen, H.H.W. Wagner, Catal. Lett. 54 (1998) 85.
[22] E.N. Jacobsen, A.R. Muci, N.H. Lee, Tetrahedron Lett. 32 (1991) 5055.
[23] J.-P. Bégué, F. Barbier, K.S. Ravikumar, D. Bonner-Delpon, Tetrahedron 54 (1998) 7457.
[24] R.A. Sheldon, I.W.C.E. Arends, M. Wallau, U. Schuchard, Acc. Chem. Res. 31 (1998) 485.